JOURNAL OF SOLID STATE CHEMISTRY **122,** 46–52 (1996)
ARTICLE NO. 0080

Crystal Structure of the New Magnetoplumbite-Related Compound in the System $SrO–Al_2O_3–MgO$

Nobuo Iyi and Matthias Göbbels*

*National Institute for Research in Inorganic Materials, Namiki 1-1, Tsukuba-shi, Ibaraki 305, Japan; and *Institut für Kristallographie, RWTH Aachen, Jägerstrasse 17-19, 52056 Aachen, Germany*

Received August 18, 1995; in revised form November 1, 1995; accepted November 8, 1995

A new phase in the system $SrO–Al_2O_3–MgO$, which was analyzed by EPMA as $Sr_2MgAl_{22}O_{36}$, was recently found. It is located in the middle of the join connecting strontium hexaaluminate ($SrAl_{12}O_{19}$) of magnetoplumbite structure and strontium magnesium hexaaluminate ($SrMgAl_{10}O_{17}$) of β-alumina structure. The crystals were grown by the floating zone method and its crystal structure was analyzed by using the single crystal X-ray was analyzed by using the single crystal X-ray diffraction method. The space group was $P\bar{6}m2$ with lattice parameters $a = 5.583$ Å and $c = 22.225$ Å. The observed c-axis length is intermediate between those of $SrAl_{12}O_{19}$ ($c = 22.00$ Å) and $SrMgAl_{10}O_{17}$ ($c = 22.399$ Å). The structure refinement result has shown that it had the alternate stacking of the conduction layers of magnetoplumbite-type ($SrAlO_3$) and β-alumina-type (SrO) separated by a spinel block ($(Al, Mg)_{11}O_{16}$). This is the first time that such a "mixed-layer" structure of β-alumina and magnetoplumbite is found to exist in the hexaaluminates containing one species of large cation.

INTRODUCTION

Hexagonal aluminates with magnetoplumbite or related structures have been known in the binary systems between alkaline earth oxides (CaO, SrO, and BaO) and Al_2O_3 (1–4). These hexaaluminates consist of so-called "conduction layers" and spinel blocks stacking alternatively in the c direction forming a layer structure (5). The difference of the conduction plane defines two types of structures, magnetoplumbite-type and β-alumina-type. In the case of the magnetoplumbite-type conduction plane, there are face-sharing AlO_6 octahedra, 12-coordinated large cations, and 5-coordinated Al ions; on the other hand, β-alumina-type structures contain corner-sharing AlO_4 tetrahedra and 9-coordinated large cations (Fig. 1). The structure refinements have revealed that Ca and Sr hexaaluminates were of magnetoplumbite-type (1–3) and Ba hexaaluminates of β-alumina-type (4, 6).

Small divalent cation Mg^{2+} is known to be incorporated in the spinel block with replacing trivalent Al^{3+} ions, and the difference of their ionic valences causes defects in the structure or sometimes modification of the structure (7). The possibility to incorporate Mg in these structures containing Ca-, Sr-, or Ba-oxides is twofold:

(i) Mg replaces Al in the Al-spinel block, inducing a valence deficiency. A charge compensation with a positively charged conduction layer is required.

(ii) A spinel unit ($Mg_2Al_4O_8$) will be inserted in the Al-spinel blocks.

For β-alumina structures (i) is preferred and (ii) is possible; on the other hand, for magnetoplumbite structures only (ii) is possible as shown, for instance, in the Al-rich part of the system $CaO–Al_2O_3–MgO$ (8) for the compounds CAM-I ($Ca_2Mg_2Al_{28}O_{46}$) and CAM-II ($CaMg_2Al_{16}O_{27}$) (9). These phases are composed of two types of structure units, M($CaAl_{12}O_{19}$; magnetoplumbite unit) and S($Mg_2Al_4O_8$; spinel unit) (10–13), and the stacking sequences are $(M_2S)_n$ for CAM-I ($c = 79.810$ Å) and $(MS)_n$ for CAM-II ($c = 31.288$ Å) (9).

As for the other divalent cations, thorough phase investigation on the Al-rich part of the system $SrO–Al_2O_3–MgO$ by Göbbels *et al.* (14) revealed the existence of the new phase, SAM-I ($Sr_2MgAl_{22}O_{36}$), in the middle of the join connecting strontium hexaaluminate ($SrAl_{12}O_{19}$, abbreviated as "SA_6") and strontium magnesium hexaaluminate ($SrMgAl_{10}O_{17}$, abbreviated as "SAM-II"). SA_6 is known to have magnetoplumbite structure (3); on the other hand, SAM-II was supposed to be of β-alumina-type (7). This indicates that the β-alumina structure is stabilized in the SrO-containing hexaaluminate system by incorporation of Mg. In contrast to the system $CaO–Al_2O_3$, where the addition of MgO did not change the magnetoplumbite structure type, the addition of MgO results in a change from the magnetoplumbite to the β-alumina structure type in the system $SrO–Al_2O_3$. Therefore the new compound SAM-I is of special interest because it represents an intermediate stage of both structure types.

To obtain samples for structural studies, single crystals

0022-4596/96 $18.00

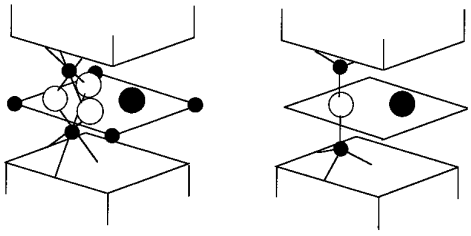

FIG. 1. Schematic representation of the conduction planes of the magnetoplumbite-type and of the β-alumina-type. Large filled circles represent the large cations, small filled circles are Al ions, and large open circles are oxygens.

TABLE 1
Crystallographic Data of Sr · Mg Hexaaluminates

	SAM-I	SAM-II
Symmetry	Hexagonal	Hexagonal
Space group	$P\bar{6}m2$	$P6_3/mmc$
Cell constants	$a = 5.583(1)$ Å	$a = 5.620(1)$ Å
	$c = 22.225(5)$ Å	$c = 22.400(2)$ Å
	$V = 599.92$ Å^3	$V = 612.57$ Å^3
	$Z = 1$	$Z = 2$
Formula[a]	$Sr_{1.86}Mg_{0.66}Al_{22.3}O_{36}$	$Sr_{0.92}Mg_{0.91}Al_{10.1}O_{17}$
Formula(ideal)	$Sr_2MgAl_{22}O_{36}$	$SrMgAl_{10}O_{17}$

[a] Experimental, by EPMA.

of these compounds, SAM-I and SAM-II, were growth by the floating zone (FZ) method and single crystal X-ray diffraction data were used for the structure refinement.

In the present paper, the crystal structures of the new compounds SAM-I and SAM-II are presented.

EXPERIMENTAL

Crystal Growth

Starting materials were high purity reagents of $SrCO_3$, MgO, and Al_2O_3 (99.9% Kojyundo Co.). They were mixed in stoichiometric ratios in an agate mortar under acetone. The homogenized batches were calcined at 1100°C to ensure the decomposition of $SrCO_3$. The hydrostatically pressed rods of suitable size were sintered in a molybdenum wound resistance furnace at 1700°C in an oxygen atmosphere. The FZ apparatus was of the infrared radiation convergence type (15) (Nichiden Machinery Ltd., NEC) using a xenon lamp as the heat source. The growth rate was 2 mm/hr in air. The resulting crystals were cut

TABLE 2
The Positional and Thermal Parameters of SAM-I

Atom	Site	Number per unit cell	Positional parameters[a]		Thermal parameters[b] × 10^4				
			x	z	U_{11}	U_{33}	U_{12}	U_{13}	B_{eq}[c]
Sr(1)	1*e*	1	2/3	0	52(5)	63(8)	$0.5U_{11}$	0	0.44(4)
Sr(2)	3*k*	0.91(1)	0.3105(12)	1/2	358(64)	95(12)	305(68)	0	1.7(5)
Al(1)	6*n*	6	0.8316(4)	0.1405(1)	18(9)	57(8)	−2(15)	−10(9)	0.28(11)
Al(2)	6*n*	6	0.1667(4)	0.35540(9)	36(9)	78(9)	19(15)	25(10)	0.39(11)
Al(3)	2*h*	2	1/3	0.2202(2)	59(12)	114(21)	$0.5U_{11}$	0	0.61(9)
Al(4)	2*i*	2	2/3	0.2729(2)	29(10)	46(15)	$0.5U_{11}$	0	0.28(7)
Al(5)	2*h*	2	1/3	0.0589(2)	26(10)	66(17)	$0.5U_{11}$	0	0.31(7)
Al(6)	2*i*	2	2/3	0.4249(2)	42(9)	16(30)	$0.5U_{11}$	0	0.39(7)
Al(7)	2*g*	2	0	0.2478(3)	37(8)	30(14)	$0.5U_{11}$	0	0.28(6)
Al(8)	2*g*	1	0	0.0100(5)	10(16)	184(72)	$0.5U_{11}$	0	0.54(21)
O(1)	6*n*	6	0.1527(7)	0.1962(2)	33(25)	62(18)	9(37)	−22(15)	0.37(25)
O(2)	6*n*	6	0.8440(7)	0.2997(2)	36(23)	33(14)	10(36)	5(17)	0.31(24)
O(3)	6*n*	6	0.5030(8)	0.1010(2)	34(20)	42(20)	10(34)	4(20)	0.31(24)
O(4)	6*n*	6	0.4949(8)	0.3988(2)	40(22)	92(22)	31(36)	−8(19)	0.41(25)
O(5)	2*i*	2	2/3	0.1917(4)	22(19)	79(35)	$0.5U_{11}$	0	0.32(14)
O(6)	2*h*	2	1/3	0.3050(4)	41(22)	61(39)	$0.5U_{11}$	0	0.38(16)
O(7)	2*g*	2	0	0.1002(4)	34(22)	42(40)	$0.5U_{11}$	0	0.29(16)
O(8)	2*g*	2	0	0.3936(6)	37(21)	72(34)	$0.5U_{11}$	0	0.38(15)
O(9)	3*j*	3	0.1807(7)	0					0.222(6)
O(10)	3*k*	1	0.6359(20)	1/2					0.67(2)

[a] $y = 2x$.

[b] $U_{22} = U_{11}$, $U_{23} = -U_{13}$. The thermal temperature factor is expressed as $\exp(-2\pi^2(h^2a^{*2}U_{11} + k^2b^{*2}U_{22} + l^2c^{*2}U_{33} + 2hka^*b^*U_{12} + 2hla^*c^*U_{13} + 2klb^*c^*U_{23})$.

[c] $B_{eq} = \frac{4}{3}(\sum_i \sum_j B_{ij}\mathbf{a}_i\mathbf{a}_j) = \frac{8}{3}\pi^2(\sum_i \sum_j U_{ij})$.

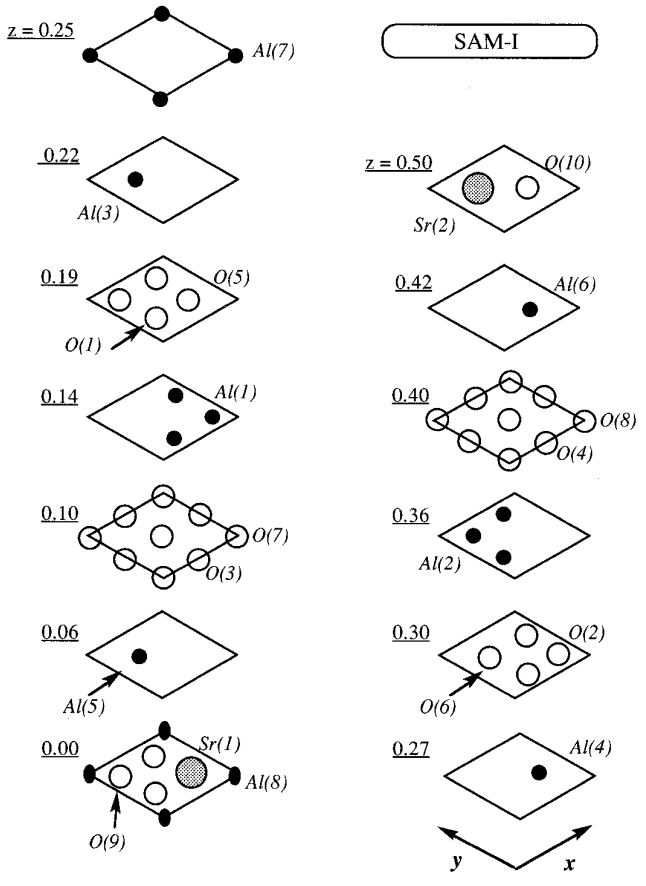

FIG. 2. The structure of SAM-I, shown in sections at various z values. The c-axis lengths of unit cells are indicated. Large filled circles represent the large cations (Sr^{2+}), small filled circles are Al ions, and large open circles are oxygens.

and prepared for EPMA (electron probe microanalysis, JEOL JXA-8600) to check the composition and for X-ray diffraction data collection.

X-Ray Data Collection

SAM-I. The selected specimen, cut from the obtained boule, was ground to a sphere with a radius of 110 μm, and was used for X-ray diffraction. The crystallinity and symmetry were checked by X-ray photographic methods. The precession and Weissenberg photos revealed that SAM-I belonged to the hexagonal crystal system. The existence of reflections with $l = 2n + 1$ for *hhl* indicates lower symmetry than $P6_3/mmc$. No evidence of superstructure was found. Specimens were mounted on a Nonius automatic four-circle diffractometer (Nonius CAD-4), and intensity was measured using graphite monochromatized Mo$K\alpha$ radiation ($\lambda = 0.71068$ Å) in a $2\theta - \omega$ scanning mode up to $2\theta = 110°$. The space group $P\bar{6}m2$ was assumed for its similarity to the magnetoplumbite structure. All reflections with $h >= 0$, $k >= 0$, $l >= 0$ were collected, and Lorenz polarization and absorption corrections were applied after the Busing and Levy algorithm (16). By using the linear absorption coefficient 57.26 cm^{-1}, the absorption due to the crystal shape was corrected. A set of 4 standard reflections was used for monitoring the fluctuation of the source X-ray intensity. The omission of the reflections with $I < 3\sigma(I)$ gave the final sets of nonzero independent reflections (a total of 1565). The $\sigma(F)$'s based on counting statistics were used for the weighing factor in the least-squares refinement ($w = 1/\sigma(F)^2$).

SAM-II. A sphere-shaped specimen with a radius of 75 μm was used for X-ray diffraction. The crystallinity and symmetry were checked by the X-ray photographic methods. The precession photos revealed that SAM-II belonged to the hexagonal crystal system with the absence of the reflections with $l = 2n + 1$ for *hhl*. So the space group $P6_3/mmc$ was assumed for this compound because of the similarity to the β-alumina structure. On the four-circle diffractometer (AFC-5, Rigaku Co. Ltd.), intensity was measured using graphite monochromatized Mo$K\alpha$ radiation ($\lambda = 0.71068$ Å) in a $2\theta - \omega$ scanning mode up to $2\theta = 120°$. The scanning speed was 1° min^{-1} in ω. All reflections of two asymmetric units were collected, and Lorenz polarization and absorption corrections were applied. The absorption due to the crystal shape was also corrected ($\mu = 58.73$ cm^{-1}). A set of 4 standard reflections was used for monitoring the fluctuation of the source X-ray intensity; however, no systematic intensity change was observed. Average of 2 equivalent reflections and omission of the reflections with $I < 3\sigma(I)$ gave the final sets of nonzero independent reflections (a total of 645), here $R\text{int} = \Sigma|F - \langle F\rangle|/\Sigma|F| = 0.016$ and $wR\text{int} = \Sigma\, w|F - \langle F\rangle|/\Sigma w|F| = 0.0095$. The $\sigma(F)$'s based on counting statistics (of equivalent reflections) were averaged and used or the weighing factor in the least-squares refinement ($w = 1/\sigma(F)^2$).

Refinement

The full matrix least-squares refinement was conducted by using the modified version of the RSFLS-4 program (17) with neutral scattering factors (18). The Fourier syntheses were done using RSSFR-5 (19). Anomalous dispersion effects of Sr and Al were taken into account for SAM-I, and the secondary extinction corrections based on the algorithm of Becker and Coppens (20, 21) were applied to the refinement of SAM-I as well as SAM-II by using the extinction parameter g (mosaic distribution).

The lattice parameters of both compounds were also determined on the basis of 20–25 reflections with a 2θ range of 50°–90° collected on the four-circle diffractometer. Here, Mo$K\alpha_1$ radiation ($\lambda = 0.70926$ Å) was used.

RESULTS AND DISCUSSION

The refinements were conducted with checking the difference Fourier maps. The final anisotropic refinement

TABLE 3
The Positional and Thermal Parameters of SAM-II

Atom	Site	Number per unit cell	Positional parameters[a]		Thermal parameters[b] × 10^4				
			x	z	U_{11}	U_{22}	U_{33}	U_{23}	B_{eq}[c]
Sr	6*h*	1.84(1)	0.6891(7)	1/4	259(15)	409(35)	95(4)	0	1.88(16)
Al(1)	12*h*	12	0.8341(1)	0.10688(3)	47(3)	46(4)	64(3)	−1(5)	0.42(3)
Al(2)	4*f*	4	1/3	0.02412(7)	69(5)	U_{11}	62(6)	0	0.53(3)
Al(3)	4*f*	4	1/3	0.17491(7)	54(5)	U_{11}	29(5)	0	0.36(3)
Al(4)	2*a*	2	0	0	53(7)	U_{11}	43(8)	0	0.39(5)
O(1)	12*k*	12	0.1537(3)	0.05222(8)	66(7)	90(12)	64(6)	−23(9)	0.56(7)
O(2)	12*k*	12	0.5055(3)	0.15003(7)	51(6)	50(9)	85(7)	−5(10)	0.49(7)
O(3)	4*f*	4	2/3	0.0596(2)	56(10)	U_{11}	107(15)	0	0.58(7)
O(4)	4*e*	4	0	0.1456(2)	48(10)	U_{11}	66(13)	0	0.43(7)
O(5)	6*h*	2	0.3085(24)	1/4	352(89)	155(87)	32(22)	0	1.59(49)

[a] $y = 2x$.
[b] $U_{12} = 1/2\ U_{22}$, $U_{13} = 1/2\ U_{23}$. The thermal temperature factor is expressed as $\exp(-2\pi^2(h^2a^{*2}U_{11} + k^2b^{*2}U_{22} + l^2c^{*2}U_{33} + 2hka^*b^*U_{12} + 2hla^*c^*U_{13} + 2klb^*c^*U_{23})$.
[c] $B_{eq} = \frac{4}{3}(\Sigma_i \Sigma_j B_{ij}\mathbf{a}_i\mathbf{a}_j) = \frac{8}{3}\pi^2(\Sigma_i \Sigma_j U_{ij})$.

converged successfully to yield $R = \Sigma||F_o| - |F_c||/\Sigma|F_o| = 0.0579$ ($wR = (\Sigma w(|F_o| - |F_c|)^2/\Sigma w|F_o|^2)^{1/2} = 0.0627$, $S = [\Sigma w(|F_o| - |F_c|)^2/(m - n)]^{1/2} = 3.69$) for SAM-I, and $R = 0.0299$ ($wR = 0.0283$, $S = 2.97$) for SAM-II. Maximum residual electron density in the final difference Fourier maps were +3.0 e/Å^3 at (1/3, 2/3, 0.17) and −3.8 e/Å^3 at (0.6, 0.4, 0.0) for SAM-I, and +1.4 e/Å^3 at (0, 0, 0) and −1.3 e/Å^3 at (0.3, 0.6, 0.03) for SAM-II. The secondary extinction parameters (g) for SAM-I and SAM-II were $0.49(8) \times 10^3$ and $6.7(2) \times 10^3$, respectively. The crystallographic data of both compounds are listed in Table 1. For SAM-I, their positional parameters, bond lengths, and angles are listed in Tables 2, 4, and 6, respectively. Tables 3, 5, and 7 show the corresponding values for SAM-II. The result showed that the structure of SAM-II is of typical β-alumina-type as has been supposed so far (7). On the other hand, SAM-I contains two types of the conduction planes, i.e., magnetoplumbite and β-alumina-types, which stack in the c direction alternately separated by normal size Al-spinel blocks (Fig. 2). In the phase diagram of the system $SrO–Al_2O_3–MgO$ (14), SAM-I is situated just in the middle of the join between SAM-II and $SrAl_{12}O_{19}$ (SA_6). SA_6 has the magnetoplumbite structure (3) and SAM-II is now confirmed to be of β-alumina-type, whereas SAM-I combines both structure types in the ratio 1 : 1. These characteristics can be also observed in the c-axis length: 22.00 Å (22) is for SA_6 and 22.399 Å for SAM-II, while the c axis of SAM-I shows an intermediate value of 22.23 Å. This fact is understandable because the c-axis length is closely related to the structure type (22).

Equilibrium study in the ternary system $SrO–Al_2O_3–MgO$ (14) shows that both phases SAM-I and SAM-II exhibit solid solution ranges to higher Al concentrations. The EPMA results of the crystals of SAM-I which were grown by the floating zone method and used for the structure determination revealed the composition to be $Sr_{1.86(4)}Mg_{0.66(9)}Al_{22.3(2)}O_{36}$ (Table 1). This means that the composition of the grown SAM-I crystal is Sr deficient compared to the ideal composition $Sr_2MgAl_{22}O_{36}$ situated just in the middle of the join of SAM-II–SA_6. Its Al-rich composition would lead to the defect of some cations to maintain charge neutrality. In fact, deficiency of Sr was observed at the Sr(2) site of SAM-I: When the occupancies at the large cation sites, Sr(1) and Sr(2), are varied during the least-square refinement, only Sr(2) in the β-alumina-type conduction plane showed the tendency to decrease in the occupancy. The obtained occupancy of Sr(2) was 0.91(1), which leads to 1.91(1) of Sr in a unit cell. This value is consistent with the Sr content of 1.86 (4) derived from EPMA. In the case of SAM-II having a typical β-alumina structure, 92% occupation of the Sr site was observed in the refinement, which is also consistent with the EPMA result as shown in Table 1. These facts indicate that vacancies are created at the large cation site of the β-alumina-type conduction plane, not at the magnetoplumbite one.

Solid solution to Al-rich side was also observed in CAM-I and -II in our previous study (8), and this phenomenon was assumed to be caused by the mechanism $3Mg^{2+}$ (sp) = $2Al^{3+}$ (sp) + □ (sp). Here, sp denotes a spinel block and □ denotes a vacancy (8, 9). According to this mechanism, the cation occupancy in the conduction layer does not change; however, it is not the case with SAM-I, and -II. The β-alumina-type Ba · Mg hexaaluminate, $Ba_{0.956}$

TABLE 4
Interatomic Distances of SAM-I

	Number of bonds	Distance (Å)
Octahedral coordination		
Al(1)–O(1)	2	1.990(5)
–O(3)	2	1.815(5)
–O(5)	1	1.960(5)
–O(7)	1	1.858(5)
Al(2)–O(2)	2	1.993(5)
–O(4)	2	1.857(5)
–O(6)	1	1.962(6)
–O(8)	1	1.822(6)
Al(5)–O(3)	3	1.889(4)
–O(9)	3	1.974(3)
Al(7)–O(2)	3	1.899(5)
–O(1)	3	1.871(5)
Tetrahedral coordination		
Al(3)–O(1)	3	1.827(2)
–O(6)	1	1.885(11)
Al(4)–O(2)	3	1.816(2)
–O(5)	1	1.804(9)
Al(6)–O(4)	3	1.759(3)
–O(10)	1	1.696(4)
Polyhedron 5-coordinated		
Al(8)–O(9)	3	1.761(2)
–O(7)	1	2.006(14)
–O(7)′	1	2.450(14)
Polyhedron 12-coordinated		
Sr(1)–O(3)	6	2.747(4)
–O(9)	6	2.795(4)
Polyhedron 9-coordinated		
Sr(2)–O(4)	3	2.685(6)
–O(4)′	3	2.871(4)
–O(10)	3	3.129(10)

$Mg_{0.912}Al_{10.09}O_{17}$, was also revealed to have similar deficiencies at the large cation site (23). In these compounds Mg + Al is nearly equal to 11. Taking the defect mechanism of Ba hexaaluminate (4) into account, a new substitution scheme $1/4\ G^{2+}(cd) + Mg^{2+}(sp) = Al^{3+}(sp) + 1/4\ \square\ (cd) + 1/4\ O^{2-}\ (cd)$ can be assumed (Type 1). Here, G denotes a large cation in the conduction plane, cd a conduction layer, and O^{2-} (cd) an interstitial oxygen in the conduction layer. In this mechanism, the small amount of vacancies at the Al site are formed because of the Frenkel-type defect. In this case, the solid solution line would extend toward the imaginary β-alumina compound "$Sr_{0.75}Al_{11}O_{17.25}$". Another possibility is $G^{2+}(cd) + 2Mg^{2+}(sp) = 2Al^{3+}(sp) + \square\ (cd)$, which will be denoted as Type 2. The difference of these two mechanisms is the existence of interstitial ions, *i*Al and *i*O, due to the "Reidinger defect" (24). When the occupancies of the Al sites are varied during the refinement of SAM-I, only Al(2) and Al(3) sites showed the decrease in the occupancy beyond 4σ. The final occupancies for Al(2) and Al(3) are 0.963(7) and 0.926(15), respectively. The occupancy of Al(3) may be due to partial replacement by the lighter ion, Mg^{2+}, as will be discussed in the next paragraph. The Frenkel-type defect shown in the β-alumina (24, 4) corresponds to the vacancy at the Al(2) site. The residual electron density at the sites expected for *i*Al and *i*O were +1.3 and +1.2 e/Å^3, respectively, for SAM-I and were +0.4 and +0.6 e/Å^3, respectively, for SAM-II. This indicates the possible presence of *i*Al and *i*O, so we can suppose that the Type 1 mechanism operates in the compounds having the β-alumina-type conduction plane. However, the residual electron densities were within the fluctuation range of the difference Fourier sections, and a very low population of these interstitial ions may have been obscured in the background electron density fluctuation in the difference Fourier synthesis. So, still there is a possibility that a mixture of the two types of mechanisms makes the Sr content vary at the same Mg content.

The Mg ions are known to occupy the tetrahedral site in the middle of the spinel block (25). Though Al and Mg can hardly be distinguished by X-ray, it would be possible to estimate at which site Mg ions are concentrated since the bond length at the tetrahedral site becomes larger when Al was replaced by Mg. Usually the Al–O bond length in a pure Al tetrahedron of the spinel block is 1.80 Å (e.g., Ref. 26), and that for $SrAl_{12}O_{19}$ is 1.797(3) Å (calculated from the data of Ref. 3). As can be seen in Table 6, Al(3)–O (average 1.84 Å) is larger than Al(4)–O (average 1.81 Å),

TABLE 5
Interatomic Distances of SAM-II

	Number of bonds	Distance (Å)
Octahedral coordination		
Al(1)–O(1)	2	1.982(2)
–O(2)	2	1.869(2)
–O(3)	1	1.944(2)
–O(4)	1	1.833(2)
Al(4)–O(1)	3	1.899(1)
Tetrahedral coordination		
Al(2)–O(1)	3	1.858(1)
–O(3)	1	1.875(4)
Al(3)–O(2)	3	1.7663(8)
–O(5)	1	1.699(2)
Polyhedron 9-coordinated		
Sr–O(2)	2	2.865(2)
–O(2)′	4	2.679(3)
–O(5)	1	3.382(4)
–O(5)′	1	3.348(12)
–O(5)″	1	3.014(12)

TABLE 6
Interatomic Angles of SAM-I

Number of bonds	Angle (°)
Octahedral coordination	
O(1)–Al(1)–O(1)′	79.98(15)
–O(3)	90.76(14)
–O(5)	90.15(20)
–O(7)	84.68(22)
O(3)–Al(1)–O(3)′	98.09(18)
–O(5)	85.43(18)
–O(7)	98.95(22)
O(2)–Al(2)–O(2)′	81.91(16)
–O(4)	92.11(15)
–O(6)	89.96(21)
–O(8)	84.77(28)
O(4)–Al(2)–O(4)′	93.54(18)
–O(6)	85.92(20)
–O(8)	98.83(27)
O(3)–Al(5)–O(3)′	97.60(22)
–O(9)	90.22(15)
O(9)–Al(5)–O(9)′	80.74(14)
O(1)–Al(7)–O(1)′	86.26(25)
–O(2)	93.41(16)
O(2)–Al(7)–O(2)′	86.92(25)
Tetrahedral coordination	
O(1)–Al(3)–O(1)′	111.82(18)
O(6)–Al(3)–O(1)	107.01(20)
O(2)–Al(4)–O(2)′	109.77(19)
–O(5)	109.17(19)
O(4)–Al(6)–O(4)′	109.70(20)
–O(10)	114.03(40)
Five coordination	
O(7)–Al(8)–O(9)	82.77(34)
–O(9)′	97.23(34)
O(9)–Al(8)–O(9)′	118.44(15)

TABLE 7
Interatomic Angles of SAM-II

Number of bonds	Angle (°)
Octahedral coordination	
O(1)–Al(1)–O(1)′	81.62(6)
–O(2)	92.43(5)
–O(3)	91.72(9)
–O(4)	84.65(8)
O(2)–Al(1)–O(2)′	93.22(6)
–O(3)	84.43(8)
–O(4)	98.84(8)
O(1)–Al(4)–O(1)′	86.03(6)
–O(1)″	93.97(6)
Tetrahedral coordination	
O(1)–Al(2)–O(1)′	109.14(7)
–O(3)	109.80(7)
O(2)–Al(3)–O(2)′	110.53(7)
–O(5)	104.17(38)
–O(5)′	110.53(7)

which indicates a more concentrated distribution of Mg at the Al(3) site than at the Al(4) site (see Fig. 2). In SAM-II (Table 5), the average bond length of Al(2)–O (the mid-spinel tetrahedral site) is 1.86 Å, indicating that Mg substitution takes place at the corresponding site.

So far, this kind of mixed layer structure, i.e., alternate stacking of β-alumina and magnetoplumbite structural units, has been known only in the case of mixed cation hexaaluminates such as Na · La hexaaluminate (27, 28). This kind of mono- and trivalent cation mixture leads to the mixed layer structure, in which Na is situated at the β-alumina-type conduction plane and La at the magnetoplumbite plane. This is also reasonable because Na hexaaluminate has β-alumina structure and La hexaaluminate has magnetoplumbite structure (29), and because the addition of the MgO component doesn't change the structure type in both cases.

The ionic radius is one of the factors determining the structure type of hexaaluminates, and the ionic radius of Sr is just at the border of the two structure types. In the case of the $CaO–Al_2O_3–MgO$ system, the hexaaluminate phases are fundamentally all based on the magnetoplumbite structure (8, 9). The ionic radius of Ca is not large enough to form β-alumina conduction planes. In contrast, Sr hexaaluminates can be incorporated in both structures, and the structure containing less vacancies would be preferred in the case of Sr; namely, $SrAl_{12}O_{19}$ of magnetoplumbite-type and $SrMgAl_{10}O_{17}$ of β-alumina-type can be formed without any vacancies. Mixed layer structure in the case of SAM-I is understandable from this point of view.

ACKNOWLEDGMENTS

The authors are very grateful to Mr. S. Takekawa (NIRIM) for his advice on the crystal growth and to Mr. K. Kosuda (NIRIM) for help in electron probe microanalysis. Travel funds from the STA (The Science and Technology Agency) of Japan for M.G. to Japan and N.I. to Germany made this work possible.

REFERENCES

1. K. Kato and H. Saalfeld, *N. Jb. Miner. Abh.* **109,** 192 (1968).
2. A. Utsunomiya, K. Tanaka, H. Morikawa, F. Marumo, and H. Kojima, *J. Solid State Chem.* **75,** 197 (1988).
3. A. J. Lindop, C. Matthews, and D. W. Goodwin, *Acta Crystallogr. Sect. B* **31,** 2940 (1975).

4. N. Iyi, Z. Inoue, S. Takekawa, and S. Kimura, *J. Solid State Chem.* **52,** 66 (1984).
5. N. Iyi, S. Takekawa, and S. Kimura, *J. Solid State Chem.* **83,** 8 (1989).
6. van Berkel, F. P. F., H. W. Zandbergen, G. C. Vershoor, and D. J. W. IJdo, *Acta Crystallogr. Sect. C* **40,** 1124 (1984).
7. A. L. N. Stevels and A. D. M. Schrama-de Pauw, *J. Electrochem. Soc.* **123,** 691 (1976).
8. M. Göbbels, E. Woermann, and J. Jung, submitted for publication.
9. N. Iyi, M. Göbbels and Y. Matsui, submitted for publication.
10. P. B. Braun, *Philips Res. Rep.* **12,** 491 (1957).
11. J. A. Kohn and D. W. Eckart, *Z. Kristallogr.* **119,** S 454 (1964).
12. R. O. Savage and A. Tauber, *J. Am. Ceram. Soc.* **47,** 13 (1964).
13. J. A. Kohn, D. W. Eckart, and C. F. Cook, Jr., *Science* **172,** 519 (1971).
14. M. Göbbels *et al.,* to be published.
15. S. Kimura and I. Shindo, *J. Crystal Growth* **41,** 192 (1977).
16. W. R. Busing and H. A. Levy, *Acta Crystallogr.* **10,** 180 (1957).
17. T. Sakurai, K. Nakatsu, H. Iwasaki, and M. Fukuhara, ''RSFLS-4, UNICS II.'' The Crystallographic Society of Japan, 1967.
18. J. A. Ibers and W. C. Hamilton, Eds., ''International Tables for X-Ray Crystallography,'' Vol 4. Kynoch Press, Birmingham, 1974.
19. T. Sakurai, ''RSSFR-5, UNICS II.'' The Crystallographic Society of Japan, 1967.
20. P. J. Becker and P. Coppens, *Acta Crystallogr. Sect. A* **30,** 148 (1974).
21. P. J. Becker and P. Coppens, *Acta Crystallogr. Sect. A* **30,** 129 (1974).
22. J. M. P. J. Verstegen and A. L. N. Stevels, *J. Lumin.* **9,** 406 (1974).
23. N. Iyi, Z. Inoue, and S. Kimura, *J. Solid State Chem.* **61,** 236 (1986).
24. W. L. Roth, F. Reidinger, and S. LaPlaca, *in* ''Superionic Conductors'' (G. D. Mahan and W. L. Roth, Eds.), p. 223. Plenum, New York, 1977.
25. G. Collin, R. Comes, J. P. Boilot, and Ph. Colomban, *Solid State Ionics* **1,** 59 (1980).
26. N. Iyi, Z. Inoue, and S. Kimura, *J. Solid State Chem.* **61,** 81 (1986).
27. J. P. Barret, D. Vivien, and J. Thery, *Mater. Res. Bull.* **18,** 59 (1983).
28. A. Kahn and J. Thery, *J. Solid State Chem.* **64,** 102 (1986).
29. N. Iyi, S. Takekawa, and S. Kimura, *J. Solid State Chem.* **54,** 70 (1984).